

Elsevier required licence: © <2020>. This manuscript version is made available under the CC-BY-NC-ND 4.0 license <http://creativecommons.org/licenses/by-nc-nd/4.0/>  
The definitive publisher version is available online at  
[\[https://www.sciencedirect.com/science/article/pii/S0048969720305258?via%3Dihub\]](https://www.sciencedirect.com/science/article/pii/S0048969720305258?via%3Dihub)

**Characterization and sulfonamide antibiotics adsorption capacity of spent coffee grounds based biochar and hydrochar**

Xinbo Zhang<sup>1,2</sup>, Yongchao Zhang<sup>1,2</sup>, Huu Hao Ngo<sup>1,3,\*</sup>, Wenshan Guo<sup>1,3</sup>, Haitao Wen<sup>1,2</sup>, Dan Zhang<sup>1,2</sup>,

Chaocan Li<sup>1,2</sup>, Li Qi<sup>1,2</sup>

<sup>1</sup> Joint Research Centre for Protective Infrastructure Technology and Environmental Green Bioprocess, School of Environmental and Municipal Engineering, Tianjin Chengjian University, Tianjin 300384, China and School of Civil and Environmental Engineering, University of Technology Sydney, NSW 2007, Australia

<sup>2</sup> Tianjin Key Laboratory of Aquatic Science and Technology, Tianjin Chengjian University, Jinjing Road 26, Tianjin 300384, China

<sup>3</sup> Centre for Technology in Water and Wastewater, School of Civil and Environmental Engineering, University of Technology Sydney, Sydney, NSW 2007, Australia

\* Correspondence author. [ngohuuhaol21@gmail.com](mailto:ngohuuhaol21@gmail.com); Tel: +61 2 9514 2745

**Abstract**

A large amount of spent coffee grounds is produced as a processing waste each year during making the coffee beverage. Sulfonamide antibiotics (SAs) are frequently detected in the environment and cause pollution problems. In this study, biochar (BC) and hydrochar (HC) were derived from spent coffee grounds through pyrolysis and hydrothermal carbonization, respectively. Their characteristics and sulfonamide antibiotics adsorption were investigated and compared with reference to adsorption capacity, adsorption isotherm and kinetics. Results showed BC possessed more carbonization and less oxygen-containing functional groups than HC when checked by Elemental Analysis, X-ray diffraction, X-ray photoelectron spectrometry and Fourier transform infrared. These groups affected the adsorption of sulfonamide antibiotics and adsorption mechanism. The maximum adsorption capacities of BC for sulfadiazine (SDZ) and sulfamethoxazole (SMX) were 121.5  $\mu\text{g/g}$  and 130.1  $\mu\text{g/g}$  at 25 °C with the initial antibiotic concentration of 500  $\mu\text{g/L}$ , respectively. Meanwhile the maximum adsorption capacities of HC were 82.2  $\mu\text{g/g}$  and 85.7  $\mu\text{g/g}$ , respectively. Moreover, the adsorption mechanism for SAs adsorbed onto BC may be dominated by  $\pi$ - $\pi$  electron donor-acceptor interactions, yet the SAs adsorption to HC may be attributed to hydrogen bonds. Further analysis of the adsorption isotherms and kinetics, found that physical and chemical interactions were involved in the SAs adsorption onto BC and HC. Overall, results suggested that: firstly, pyrolysis was an effective thermochemical conversion of spent coffee grounds; and secondly, BC was the more promising adsorbent for removing sulfonamide antibiotics.

**Keywords:** spent coffee grounds; biochar; hydrochar; sulfonamide antibiotics; adsorption

## 1. Introduction

Coffee is one of the most popular beverages drunk worldwide and it is brewed from roasted beans. On average, about one kilogram of soluble coffee can produce two kilograms of wet spent coffee grounds (Tsai, 2017). According to one estimation published by the International Coffee Organization, the global consumption of coffee exceeded 9.3 billion kilograms in 2016 (McNutt and He, 2019). There is no corresponding market demand for currently used spent coffee grounds, and this subsequently creates disposal problems. Most spent coffee grounds are simply landfilled and incinerated, resulting in wasted resources and environmental pollution (Li et al., 2014). However, spent coffee grounds do represent a potential resource because of its high organic content, containing for example, hemicellulose, cellulose, lignin and protein (Tsai, 2017). Spent coffee grounds have been investigated for their valorization, such as their complete utilization to produce biodiesel, bio-oil, and biochar (Vardon et al., 2013). Biochar has been used as a carbonaceous material for removing many contaminants such as antibiotics (Ahmed et al., 2015), heavy metals (Bakshi et al., 2018) and dyes (Chen et al., 2018), due to the biochar's rich surface functional groups and porous structure.

In addition, antibiotics are extensively used in human and animal medicine, animal husbandry and agriculture, which has led to their continuous and damaging release into the environment and subsequent development and dissemination of



antibiotics-resistant genes (Almakki et al., 2019; Li et al., 2019b). Some reports in recent years have focused on how to remove antibiotics by phase-changing, which includes adsorption in different solid matrices and membrane processes. This strategy is followed by biological treatment and advanced oxidation processes (Rodriguez-Narvaez et al., 2017), where adsorption is one of the best cost-effective methods to remove antibiotics. Biochar can function as an important adsorbent for the removal of antibiotics because of its high removal rate (Ahmed et al., 2015). Of the studies done on adsorptive removal of sulfamethazine on biochar, it was reported that tea waste biochar had a high adsorption capacity (33.81 mg/g) using steam-activated biochar produced at 700°C (Rajapaksha et al., 2014). Hardwood biochar exhibited a high adsorption distribution ratio value ( $10^6$  L/kg) for the removal of sulfamethazine (Teixido et al., 2011). Spent coffee grounds biochar (pyrolysis at 500°C) had a high adsorption capacity (39.22 mg/g) for tetracycline adsorption (Nguyen et al., 2019).

According to previous reports, the characteristics of biochar greatly depend on the process parameters including reaction temperature, reaction time, feedstock, heating rate, etc. (Wang et al., 2018). Moreover, production methods also play a critical role in characteristics of biochar (Yu et al., 2017). Biomass is converted into biochar through different production methods such as pyrolysis and hydrothermal carbonization (HTC). There are many reports about the biochar characteristics or adsorption behavior of biochar produced by a single production method (Heo et al., 2019; Liu et al., 2018; Liu et al., 2019; Zhang et al., 2019a). However, to date, few

studies have been conducted on a comparison of characteristics and adsorption behaviors of the biochar produced by different production methods. This study aims to compare the characterization of carbonaceous material prepared by pyrolysis and HTC under different production conditions, as well as the adsorption of sulfonamide antibiotics (SAs). Furthermore adsorption isotherms and adsorption kinetics were used to explore the adsorption process of SAs.

## **2. Materials and methods**

### **2.1 Materials and chemicals**

Spent coffee grounds with an average moisture content of 60% were collected from a Starbucks outlet in Tianjin, China. Sulfadiazine (SDZ) and sulfamethoxazole (SMX) were selected in the SAs adsorption experiments, and their characteristics are shown in **Table 1**. SDZ and SMX were purchased from Tianjin Heowns Biochem LLC. Formic acid was purchased from Tianjin Damao Chemical Reagent Factory. Methanol and acetonitrile were obtained from Thermo Fisher Scientific. Ammonium formate was obtained from Tianjin Naikai Share Compounds Co., Ltd. All chemicals or reagents employed for the experiments conducted in this study were of analytical grade or higher.

#### **Table 1.**

## 2.2 Biochar and hydrochar preparation

The conversion of spent coffee grounds into solid carbonaceous products was carried out by pyrolysis and HTC, and these products were named biochar (BC) and hydrochar (HC), respectively. Processes involved are explained in more detail below.

The spent coffee grounds were dried in natural conditions and dried in an oven at 105°C for 24 h. BC was prepared via the pyrolysis of spent coffee grounds through a muffle furnace, which was operated for 2 h at 200°C, 300°C, 400°C, 500°C, 600°C, 700°C under limited oxygen, while the pyrolysis heating rate was set at 5°C /min. To eliminate inorganic components, the obtained biochar products were treated by washing them with a mixture of 1 M HCl, and then they were washed several times with distilled water until all residual acid was removed. The product made under 200°C was designated as BC-200. Similarly, other products were recorded as BC-300, BC-400, BC-500, BC-600, and BC-700 according to the reaction temperature (300°C, 400°C, 500°C, 600°C and 700°C). HC was prepared by hydrothermal carbonization of spent coffee grounds, which were subjected to production at 2 h, 4 h, 6 h, 8 h, 10 h, and 12 h at 160°C by hydrothermal synthesis reactor; the water to raw material ratio was 1:10. The solid product was collected by vacuum filtration, washed with deionized water until the pH of the washed water achieved a stable state, and dried at 105°C for 12 h. HC was marked in accordance with residence time (2 h, 4 h, 6 h, 8 h, 10 h and 12 h), and recorded as HC-2, HC-4, HC-6, HC-8, HC-10, and HC-12, respectively. All samples were sieved with a 100 mesh sieve ( $\leq 0.15\text{mm}$ ).

### 2.3 Characterization of BC and HC

The carbon, hydrogen and nitrogen contents of BC and HC were measured with an elemental analyzer (vario EI cube, Germany). Ash contents were determined by burning samples at 800°C for 4 h. The oxygen content was calculated from the mass conservation equilibrium (1).

$$O (\%) = 100 (\%) - C (\%) - H (\%) - N (\%) - \text{Ash} (\%) \quad (1)$$

Where O, H, N and Ash constitute the proportion of oxygen, hydrogen, nitrogen and ash content in the mass of BC or HC, respectively.

Thermogravimetric analysis (TGA, STA449F3, Germany) was used for examining the relationship between the quality of spent coffee grounds and temperature changes.

Scanning electron microscopy (SEM, JSM-7800F, Japan) images were generated to understand the surface morphology of the sample. Fractions of the structure were assessed by X-ray diffraction (XRD) measurements with a D8 ADVANCE X-ray diffractometer (Germany). The XRD experiments were carried out with a  $2\theta$  range of  $10^\circ$ - $80^\circ$ . The functional groups of BC and HC were obtained by Fourier transform infrared (FTIR, Is10, US) spectroscopy. X-ray photoelectron spectrometry (XPS) (K-alpha, USA) was used to analyze the surface functionalities of BC and HC.

Brunauer–Emmett–Teller (BET), total pore volumes and pore diameters were evaluated using  $N_2$  adsorption/desorption isotherms that were determined at 77.35 K using a surface area and porosity analyzer (Tristar II 3020, USA) after vacuum degassing at 378 K for 5 h.

## 2.4 Adsorption experiments

Batch experiments were conducted in the adsorption experiments of SAs to BC or HC to evaluate the effectiveness in removing SAs. First, reaction solutions were prepared with SAs in deionized water in 0.1% methanol at pH  $6.8 \pm 0.2$ . 100 mg of sample (BC or HC) and 30 mL solution (SDZ or SMX,  $500 \mu\text{g/L}$ ) were placed in a 50 mL sealed conical flask. Subsequently, the sealed conical flask was placed in a shaker and shaken at 150 rpm and  $25^\circ\text{C}$  for 24 h. After shaking, the mixed solutions from the shaker were filtered with a  $0.22 \mu\text{m}$  Luer Syringe Filter and then determined following the solid phase extraction phase. All the samples were conducted in duplicate.

## 2.5 Adsorption isotherm

To further explore the mechanism of adsorption, the adsorption isotherm was established to describe the relationship between SAs and BC (HC). The BC and HC, which exhibited the largest adsorption capacities of SDZ and SMX, were selected for the adsorption isotherms tests. These adsorption isotherm experiments explored the adsorption mechanism as follows. Firstly, 100 mg of the sample was mixed with 5, 10, 20, 50, 100, 200, 500, 1000, 2000  $\mu\text{g/L}$  concentrations of SAs in a shaker at 150 rpm and  $25^\circ\text{C}$  for 24 h. Three replicates were then taken out of the shaker for analysis. To further analyze the experiment data, Langmuir and Freundlich isotherm models were used as adsorption isotherm models in this research study as they can be applicable to

describe multilayer adsorption on a heterogenous surface and monolayer adsorption on a homogenous surface, respectively. The relationship between the adsorption concentration ( $C_e$ ) and adsorption capacity ( $Q_e$ ) was described utilizing the Langmuir and Freundlich equilibrium isotherm models. The Langmuir isotherm model was described as follows:

$$Q_e = Q_m K_L C_e / (1 + K_L C_e) \quad (2)$$

Where  $C_e$  is equilibrium aqueous-phase concentration of sulfonamides ( $\mu\text{g/L}$ ),  $Q_e$  is the adsorption capacity of sulfonamides ( $\mu\text{g/g}$ ),  $Q_m$  is the maximum adsorption capacity of sulfonamides ( $\mu\text{g/g}$ ), and  $K_L$  is the Langmuir constant ( $\text{L}/\mu\text{g}$ ).

The Freundlich isotherm model was described as follows:

$$Q_e = K_F C_e^n \quad (3)$$

Where  $K_F$  is the Freundlich adsorption capacity parameter, and  $n$  is the Freundlich constant, which is related to the heterogeneity factor.

## 2.6 Adsorption kinetics

To investigate the effect of adsorption time on the SAs to BC or HC, adsorption kinetic experiments were conducted. Initially, 100 mg of BC (HC) sample and 30 mL of the SAs solutions ( $500 \mu\text{g/L}$ ) was placed in a 50 mL conical flask and shaken at 150 rpm at  $25^\circ\text{C}$  for 72 h. At the time intervals of 0.5, 2, 5, 10, 16, 24, 36, 48 and 72 h, three replicates were taken out of the flask for analysis. In order to explain the adsorption mechanism, a variety of kinetic model which included the pseudo-first order model and pseudo-second order model were used to fit the kinetics data

regarding the sulfonamide antibiotics adsorption on BC or HC. The models were described as follows:

$$\text{Pseudo-first order model: } q_t = q_e(1 - e^{-k_1 t}) \quad (4)$$

$$\text{Pseudo-second order model: } q_t = k_2 q_e^2 t / (1 + k_2 q_e t) \quad (5)$$

Where  $q_t$  is the adsorption capacity at time  $t$  ( $\mu\text{g/g}$ ),  $q_e$  is the adsorption capacity at equilibrium ( $\mu\text{g/g}$ ),  $k_1$  is the rate constant of the first-order kinetic equation ( $\text{h}^{-1}$ ),  $k_2$  is the rate constant of the pseudo-second-order kinetic equation ( $\text{g } \mu\text{g}^{-1} \text{h}^{-1}$ ), and  $t$  is contact time (h).

## 2.7 Determination of sulfonamide antibiotics

The SAs samples was analyzed by liquid chromatography and tandem mass spectrometry (LC-MS/MS). The LC-MS/MS system (Agilent 1200 Series) was equipped with an Agilent Eclipse C18 column (diameter, length and aperture of 2.1 mm, 150 mm, 3.5  $\mu\text{m}$ , respectively). The mobile phase for determining SAs was a mixture solution containing 0.01 mol/L ammonium formate water with 0.1% formic (Solvent A)/acetonitrile (solvent B) = 80/20 (v/v). The injection volume of the sample was 5  $\mu\text{L}$  and the flow rate was 0.4 mL/min with the (A/B) constant gradient when separation was achieved at 35°C. The system's total run time was 3 min and equilibrated for 5 min before the next injection was done. Within the concentration range of the experiments, the correlation coefficient ( $R^2$ ) of the standard curve generated after calibration was greater than 0.99. The retention times, parent ions, daughter ions, limit of detection (LOD), limit of quantification (LOQ) of SDZ and

SMX were listed in **Table 2**.

**Table 2.**

### **3. Results and discussion**

#### **3.1 Characterization of BC and HC**

##### **3.1.1 Yield, elemental composition and ash content**

The yield, elemental composition and ash content of BC and HC are listed in **Table 3**. Yields of HC were in the 64.5%-80.3% range, which was higher than BC except BC-200 (96.8%), and this was related to the thermal and combustion behavior of spent coffee grounds. The thermal and combustion behavior of pyrolysis can be reflected in the thermogravimetric analysis (**Fig. 1**). The decomposition process of the spent coffee grounds comprised three discrete stages. Below the temperature of 220°C, the first stage of decomposition of the spent coffee grounds corresponded to the evaporation of adsorbed water in the sample (Kelkar et al., 2015), resulting in a high yield of BC-200. Referring to the second stage of 220-500°C, the main complex reactions led to the most significant mass loss, such as hemicellulose, cellulose and lignin which were all decomposed. In the third stage when conditions were above 500°C, the residual solids were slightly weightless due to char consolidation. In the HTC process, the use of different reaction mediums led to different amounts of decomposition of the components in the coffee grounds. For example, most of the lignin remained during the HTC process (Kambo and Dutta, 2015). This resulted in a



high yield of HC which actually had less carbon content (55.82-59.99 % versus 68.82-81.23%) but higher surface oxygen (28.74-32.14% versus 9.81-19.76%) compared to BC except BC-200 (49.66% for carbon, 40.11% for oxygen), which indicated that BC exhibited a higher degree of carbonization and more aromatic structures. The ash percentage of HC varied from 0.30% to 0.70%, which was lower than that of BC (0.3-4.55%). This was due to the presence of compressed liquid in the HTC process that gave aid to the demineralization of ash composition in the spent coffee grounds, resulting in the reduction of ash content (Kambo and Dutta, 2015). The molar ratios of O/C, H/C, and (N+O)/C represented the hydrophobicity, aromaticity and polarity of BC and HC, respectively (Rajapaksha et al., 2014). Compared to HC, BC (except BC-200) had a lower ratio of O/C (from 0.12 to 0.29), H/C (from 0.12 to 0.11), and (N+O)/C (from 0.16 to 0.33). These results suggested that BC had higher hydrophobicity, aromaticity and lower polarity.

**Fig. 1.**

**Table 3.**

### 3.1.2 Pore properties of BC and HC

From the data shown in **Table 3**, the specific surface area (BET) and pore volume of BC increased first and then decreased with the increasing temperature. The relatively low temperature favored the formation of pores, while a higher temperature (>400°C) caused the pores to be destroyed. Meanwhile, the decline in the pores existing in the BC could be observed by scanning electron microscopy images at a

high temperature more than 400°C (**Fig. 2**). In the meantime the BET and pore volume of HC increased with the reaction time. Consequently, the reaction time favored the formation of BET and pore volume in the HTC process. BC had a relatively larger BET and pore volume than HC (**Table 3**), which were also reflected in the scanning electron microscopy images of BC and HC (**Fig. 2**).

**Fig. 2.**

### 3.1.3 XRD and surface functional groups

From the XRD patterns of BC and HC (**Fig. 3a**), broad peaks with  $2\theta$  at around  $24^\circ$  appeared on the BC-400 and BC-500, suggesting the presence of an ordered graphitic structure (Xie et al., 2014). A diffraction peak at  $2\theta$  of  $20^\circ$  of HC-6h and HC-10h was detected, which was ascribed to the presence of crystalline sucrose (Nguyen et al., 2019). The differences in diffraction peaks between BC and HC were explained by the BC having more carbonization.

Surface functional groups, especially O-containing functional groups, could assist chemical or semi-chemical adsorption for organics on the BC and HC (Li et al., 2019c). Further insights into the functional groups of BC and HC were obtained by FTIR (**Fig. 3**). It can be seen that BC and HC shared some of the same functional groups, for instance O-H (between 3300 and 3800  $\text{cm}^{-1}$ ), C-H (between 2845 and 2970  $\text{cm}^{-1}$ , around 1384  $\text{cm}^{-1}$ ), C=C (between 1630 and 1640  $\text{cm}^{-1}$ ), and C-O (between 1000 and 1100  $\text{cm}^{-1}$ ). In BC-200, BC-300 and HC, there is also a same broad band at between 1660 and 1760  $\text{cm}^{-1}$ , which was consistent with C=O group.

When compared the spectra of BC and HC, it was observed that the peak intensity of HC lay between: firstly, 1550 and 1600  $\text{cm}^{-1}$  indicating the -COOH group; and secondly, around 1163  $\text{cm}^{-1}$  indicating the C-O-C group. Yet they were not observed in the BC sample. It was suggested that HC had more oxygen-containing functional groups, and this finding proved to be consistent with the elemental composition analysis that confirmed more oxygen on the HC (shown in **Table 3**). Therefore HC had higher hydrophilicity than BC (Li et al., 2018).

**Fig. 3.**

The xps spectra also showed that HC had a higher content of oxygen-containing functional groups than BC (**Fig. 4**). The C1s spectra of BC-400, BC-500, HC-6h and HC-10h was deconvoluted into three peaks at 284.8, 286.5 and 288.4 eV, which were assigned to C-C, C-O, and C=O or O-C-O, respectively. As shown in **Fig. 4**, the molar of C-O, and C=O or O-C-O of BC-400 (11.64% and 6.97%, respectively) and BC-500 (11.41% and 4.22%, respectively) was lower than that of HC-6h (18.63% and 9.41%, respectively) and HC-10h (12.91% and 8.59%, respectively).

**Fig. 4.**

### 3.2 Adsorption of sulfonamide antibiotics to BC and HC

The adsorption capacities at an initial concentration of 500  $\mu\text{g/L}$  for SDZ and SMX are depicted in **Fig. 5**, which exhibited the removal of SAs from BC and HC. The adsorption capacities of SDZ and SMX on the different BC ranged from 17.7 to 121.5  $\mu\text{g/g}$ , 21.2 to 130.1  $\mu\text{g/g}$ , respectively. In contrast, for the HC, its adsorption

capacities of SDZ and SMX varied from 43.4 to 82.2  $\mu\text{g/g}$ , 36.1 to 85.7  $\mu\text{g/g}$ , respectively. It can be seen in **Fig. 5** that BC possessed a higher maximum adsorption capacity than HC, indicating BC was better as an adsorbent for removing SAs from wastewater. The adsorption of the biochar on the organic solvents was a function of the surface and bulk properties of carbonization and non-carbonization aspects of the biochar (Zhang et al., 2019b). Since both BC and HC displayed different adsorption capacities for SDZ and SMX, the combined effects of several mechanisms may be involved in the adsorption process.

It was well documented in the literature that the adsorption of SAs was attributed to various mechanisms, namely,  $\pi$ - $\pi$  electron donor-acceptor (EDA) interactions, hydrogen bonds, van der Waals forces, hydrophobicity and pore-filling (Ahmed et al., 2017; Li et al., 2019a; Sun et al., 2018). Now that BC and HC presented the various forms and amounts in the carbonized and non-carbonized parts, this explained the differences in their dominant adsorption mechanisms. It is known that HC has relatively less carbonization and more content of amorphous domains, polarity, and functionality (**Table 3**). Consequently, hydrogen bonds played a more important role in SDZ and SMX adsorption on HC. This was confirmed by the FTIR spectra that are presented in **Fig. 3d**, and they show that the carboxyl group around  $1163\text{ cm}^{-1}$  disappeared after the adsorption reaction of HC with SDZ and SMX. It indicated a possible adsorption mechanism involving hydrogen bonds between the SDZ (SMX) and the carboxyl group (Lian et al., 2015). In contrast, BC developed a large amount

of graphitic-like fractions (**Fig. 3a**) but contained less polar domains and functionality (**Table 3**). Both SDZ and SMX molecules had strong  $\pi$ -acceptors due to their amino functional group and N-heteroaromatic ring (Kah et al., 2017). Therefore, the graphitic carbon surface area ( $\pi$ -donor) largely dominated the adsorption of SDZ and SMX by BC via  $\pi$ - $\pi$  electron donor-acceptor.

BC and HC exhibited different adsorption capacities for SDZ and SMX under the same adsorption experiment conditions. The maximum adsorption capacities of SDZ and SMX were obtained in BC-500 and BC-400, respectively. For HC, its maximum adsorption capacities of SDZ and SMX were obtained in HC-10 h and HC-6 h, respectively. The different adsorption capacities of BC and HC were linked to particular properties of SDZ and SMX themselves (**Table 1**). These key chemical properties, specifically octanol-water partitioning coefficient ( $K_{ow}$ ), acidity constant ( $pK_a$ ) and molar refractivity, played major roles in assessing the adsorption behavior of different SAs. The octanol-water partitioning coefficient ( $K_{ow}$ ) was commonly used as an indicator of the adsorbate's hydrophobicity. Acidity constant ( $pK_a$ ) was related to the speciation of SAs. Molar refractivity had a certain correlation with van der Waals forces (Sun et al., 2018). As reported in previous studies, the adsorption of different SAs on biochar was due to several factors, such as van der Waals forces and hydrophobicity (Sun et al., 2018). Similarly, the capacities of these two different SAs under the same conditions were resulted from a combination of multiple forces.

In this study, because SDZ had higher  $K_{ow}$  than SMX, hydrophobicity can play a more important role in the adsorption of SDZ for BC and HC. Moreover, from the perspective of species of SDZ and SMX, more than 94% of SMX molecules ( $pK_{a,2}=5.7$ ) were negatively charged at pH of  $6.8 \pm 0.2$ , while SDZ molecule ( $pK_{a,2}=6.5$ ) existed in more neutral species. Since neutral molecules can be more strongly adsorbed on BC and HC than negatively charged molecules (Lian et al., 2015), SDZ can be better adsorbed on BC and HC. However, van der Waals forces may be stronger in the SMX adsorption process for BC and HC, on account of SMX's higher molar refractivity than SDZ.

As well, electrostatic interactions can affect the adsorption of ionic compounds (Peiris et al., 2017). The surface areas of BC and HC exhibited a negative charge. The electrostatic repulsion between anions and negatively charged BC or HC could inhibit adsorption. However, both BC and HC continued to display a capacity to adsorb large amounts of SDZ and SMX, other factors might facilitate their adsorption. In a previous study, charge assisted hydrogen bonding made a major contribution to the reaction between SMX and biochar (Lian et al., 2015). A possible explanation for higher adsorption capacity between anions and BC (HC) was that charge assisted hydrogen bonding interactions were likely one of the major interactions to occur.

**Fig. 5.**

### **3.3 Adsorption isotherms**

The adsorption isotherms for two kinds of SAs in both BC and HC are shown in

**Fig. 6.** It can be seen that both Freundlich and Langmuir models fit to the SDZ and SMX adsorption isotherms well with regression coefficients of  $r^2 > 0.93$  (**Table 4**). The experimental data were better fitted to the Langmuir model due to the higher  $r^2$  values except for SMX adsorption of BC, indicating that the adsorption process followed a reversible monolayer adsorption mechanism. The  $Q_m$  values derived from the Langmuir model were 295.1, 740.6  $\mu\text{g/g}$  for SDZ and SMX on selected HC, respectively, which proved to be higher than BC (221.9  $\mu\text{g/g}$  for SDZ and 481.6  $\mu\text{g/g}$  for SMX).

The  $K_L$  value can help to identify different adsorbents and reflect the affinity or bond strength between the adsorbent and adsorbate. There was a stronger affinity or bonding strength between BC and two kinds of SAs ( $K_L(\text{BC}) > K_L(\text{HC})$ ). In addition, the Freundlich isotherm model provided a better fit for SMX adsorption to BC, which meant that the adsorption of BC and SMX was a multilayer adsorption of energy unevenly distributed on the heterogeneous surface. Its adsorption ability was able to increase when the adsorbate concentration also increased. All of the Freundlich parameter  $n$  values were less than 1 (**Table 4**), suggesting that a favorable adsorption process for two kinds of SAs on the BC and HC was possible.

Furthermore, the standard Gibbs free energy ( $\Delta G_0$ ) of adsorption was calculated based on the Van't Hoff equation (Naga Babu et al., 2018). The negative  $\Delta G_0$  changes of SDZ and SMX adsorption confirmed that the sorption process was spontaneous (**Table 5**). The  $\Delta G_0$  was in the  $-0.48$  to  $-4.65$  kJ/mol range, indicating that the process

of physical adsorption was involved in the adsorption process of SDZ and SMX.

**Fig. 6.**

**Table 4.**

### 3.4 Adsorption kinetics

The adsorption kinetic parameters and curve fits are shown in **Table 5** and **Fig. 7**.

It is known that the pseudo-first order model was based on the assumption that the adsorption was controlled by diffusion steps. The pseudo-second order model assumed that: firstly, the adsorption rate was determined by the square of the adsorption site vacancies on the adsorbent surface; and secondly, the adsorption process was controlled by the chemisorption mechanism. As the adsorption kinetic parameters, the pseudo-second order model had a relatively high correlation coefficients ( $r^2$ ) values for SAs on the BC and HC, indicating that chemical adsorption controlled the adsorption process. The chemisorption involved valency forces through sharing or exchange of electrons between BC (HC) and SAs, such as covalent forces (Jia et al., 2013). As shown in **Fig. 7**, the adsorption of SDZ and SMX could be structured into a 3-stage reaction process involving rapid adsorption, slow adsorption and equilibrium. During the rapid adsorption phase, the adsorption of SMX could occur rapidly within 5h, while the adsorption of SDZ underwent a relatively slow adsorption process (16h). Subsequently, both SMX and SDZ were subjected to a slow adsorption process until the adsorption equilibrium was reached.

It appeared that 3 stages may be involved in the active adsorption sites on BC



and HC (Zhang et al., 2019a). In the first stage, there were abundant active adsorption sites on both the BC and HC, which led to rapid adsorption. As the reaction progressed, the gradual decrease in the number of free adsorption sites of BC or HC led to a slowing down in the adsorption, i.e. the second stage. The third stage was the adsorption equilibrium, which may have been due to two things: firstly, the decline in free adsorption sites on the BC and HC; and secondly, an increase in electrostatic repulsion between the SAs molecules adsorbed on the BC or HC surface and SAs molecules in the solution. Getting the data to fit the pseudo-second order kinetics model, the rate constant ( $k_2$ ) of SMX was greater than that of adsorbed SDZ (**Table 5**), which suggested that the adsorption of SMX was faster than SDZ adsorption.

**Fig. 7.**

**Table 5.**

### **3.5 Techno-economic feasibility**

#### **3.5.1 Technical feasibility**

At the current level of technology from this study, the production of BC and HC can be achieved. There are already some data of available technology for industrial-scale HTC. For example, TerraNova Energy uses 8000 tons of wet sludge as raw material each year to perform HTC of 200 °C for 4h ([http:// www.terranova-energy.com](http://www.terranova-energy.com)). In addition, compared to the production process of activated carbon, the production temperature of BC and HC is lower, and no activation

treatment is required during the production process.

### 3.5.2 Economic feasibility

The production cost of BC and HC is an important factor determining whether they can practically be used. Base on this, the total production cost of BC and HC was estimated and calculated by Eq. (6).

The total production cost =collecting raw materials cost + production cost + additional cost (6)

The cost of producing 1kg of spent coffee grounds BC and HC was estimated as follow:

The collecting raw materials cost including raw material cost, transportation cost and storage cost is about 4 CNY (~ USD \$ 0.58). Production cost is mainly the cost of electricity consumption during the production process. The electricity used is mainly generated during drying and pyrolysis (HTC) process. Therefore, the production cost for BC and HC is about 23.8 CNY (~ USD \$ 3.47) and 22.5 CNY (~ USD \$ 3.28), respectively. Addition cost include labor cost, equipment maintenance cost and packaging cost, etc. The estimated cost the part is 17.5 CNY (~ USD \$ 2.55).

Hence, the total cost of producing 1kg of spent coffee grounds BC and HC is 45.3 CNY (~ USD \$ 6.60) and 48.7 CNY (~ USD \$ 6.41) respectively. Obviously, both BC and HC are cheaper than commercial activated carbon (up to \$11.59/kg, Fujian Xinsen Carbon Industry Co., Ltd).

Although spent coffee grounds BC and HC are proved to be techno-economic feasibility, it is still some challenges to use biochar-based systems for large-scale applications in real wastewater. In reality, some aspects need to be fully considered, including (i) the impact of competitive adsorption due to the complexity of the actual wastewater composition; (ii) there is no uniform standard to evaluate the quality of biochar; (iii) the lack of understanding of adsorption mechanism in adsorption process makes it impossible to judge whether the application will cause secondary pollution. Relatively speaking, biochar is a unique resource with great potential to solve some practical problems such as (i) remediation of pollutants in soil, water, and gaseous media; (ii) improve soil, water and air quality; (iii) carbon sequestration and greenhouse gas emissions mitigation.

#### **4. Conclusion**

The physical and chemical characteristics and adsorption performance of biochar were affected by production methods. Compared to HC, BC exhibited higher carbon content, hydrophobicity and aromaticity, lower polarity and less oxygen-containing functional groups. By evaluating the adsorption of sulfonamide antibiotics to BC and HC, BC showed greater maximum adsorption capacity, which suggested that BC was more suitable as an adsorbent for adsorptive removal of sulfonamide antibiotics from wastewater. After mechanism analysis, the interaction of  $\pi$ - $\pi$  donor acceptor may be predominant in the adsorption of sulfonamide antibiotics on BC, while hydrogen

bonds may play a more important role in the adsorption process for HC. The adsorption data of SMX (SDZ) and BC (HC) were better fitted to the Langmuir model except for SMX adsorption of BC. The pseudo-second order model could well describe the SAs adsorption kinetics on BC and HC. After the techno-economic feasibility analysis, the content of this research is feasible, but considering the practical problems, it still need to be explored.

### **Acknowledgements**

The work was supported by Tianjin Municipal Science and Technology Bureau of China (Project No. 18PTZWHZ00140) and Ministry of Science and Technology of China (Project No. 2017ZX07107-001-003).

### **References**

- Ahmed MB, Zhou JL, Ngo HH, Guo W. Adsorptive removal of antibiotics from water and wastewater: Progress and challenges. *Sci. Total Environ.* 2015; 532: 112-26.
- Ahmed MB, Zhou JL, Ngo HH, Guo W, Johir MAH, Sornalingam K. Single and competitive sorption properties and mechanism of functionalized biochar for removing sulfonamide antibiotics from water. *Chem. Eng. J.* 2017; 311: 348-358.
- Almakki A, Jumas-Bilak E, Marchandin H, Licznar-Fajardo P. Antibiotic resistance in urban runoff. *Sci. Total Environ.* 2019; 667: 64-76.

- Bakshi S, Banik C, Rathke SJ, Laird DA. Arsenic sorption on zero-valent iron-biochar complexes. *Water Res.* 2018; 137: 153-163.
- Chen YD, Lin YC, Ho SH, Zhou Y, Ren NQ. Highly efficient adsorption of dyes by biochar derived from pigments-extracted macroalgae pyrolyzed at different temperature. *Bioresour. Technol.* 2018; 259: 104-110.
- Heo J, Yoon Y, Lee G, Kim Y, Han J, Park CM. Enhanced adsorption of bisphenol A and sulfamethoxazole by a novel magnetic CuZnFe<sub>2</sub>O<sub>4</sub>-biochar composite. *Bioresour. Technol.* 2019; 281: 179-187.
- Jia M, Wang F, Bian Y, Jin X, Song Y, Kengara FO, et al. Effects of pH and metal ions on oxytetracycline sorption to maize-straw-derived biochar. *Bioresour. Technol.* 2013; 136: 87-93.
- Kah M, Sigmund G, Xiao F, Hofmann T. Sorption of ionizable and ionic organic compounds to biochar, activated carbon and other carbonaceous materials. *Water Res.* 2017; 124: 673-692.
- Kambo HS, Dutta A. A comparative review of biochar and hydrochar in terms of production, physico-chemical properties and applications. *Renew. and Sustainable Energy Reviews* 2015; 45: 359-378.
- Kelkar S, Saffron CM, Chai L, Bovee J, Stuecken TR, Garedew M, et al. Pyrolysis of spent coffee grounds using a screw-conveyor reactor. *Fuel Process. Technol.* 2015; 137: 170-178.
- Li C, Zhu X, He H, Fang Y, Dong H, Lü J, et al. Adsorption of two antibiotics on

- biochar prepared in air-containing atmosphere: Influence of biochar porosity and molecular size of antibiotics. *J. Mol. Liquids* 2019a; 274: 353-361.
- Li S, Zhang R, Hu J, Shi W, Kuang Y, Guo X, et al. Occurrence and removal of antibiotics and antibiotic resistance genes in natural and constructed riverine wetlands in Beijing, China. *Sci. Total Environ.* 2019b; 664: 546-553.
- Li X, Strezov V, Kan T. Energy recovery potential analysis of spent coffee grounds pyrolysis products. *J. Analytical and Appl. Pyrolysis* 2014; 110: 79-87.
- Li Y, Meas A, Shan S, Yang R, Gai X, Wang H, et al. Hydrochars from bamboo sawdust through acid assisted and two-stage hydrothermal carbonization for removal of two organics from aqueous solution. *Bioresour. Technol.* 2018; 261: 257-264.
- Li Y, Tsend N, Li T, Liu H, Yang R, Gai X, et al. Microwave assisted hydrothermal preparation of rice straw hydrochars for adsorption of organics and heavy metals. *Bioresour. Technol.* 2019c; 273: 136-143.
- Lian F, Sun B, Chen X, Zhu L, Liu Z, Xing B. Effect of humic acid (HA) on sulfonamide sorption by biochars. *Environ. Pollut.* 2015; 204: 306-12.
- Liu F, Yu R, Ji X, Guo M. Hydrothermal carbonization of holocellulose into hydrochar: Structural, chemical characteristics, and combustion behavior. *Bioresour. Technol.* 2018; 263: 508-516.
- Liu H, Chen Y, Yang H, Gentili FG, Söderlind U, Wang X, et al. Hydrothermal carbonization of natural microalgae containing a high ash content. *Fuel* 2019;

249: 441-448.

McNutt J, He Q. Spent coffee grounds: A review on current utilization. *J. Industrial and Eng. Chem.* 2019; 71: 78-88.

Naga Babu A, Reddy DS, Kumar GS, Ravindhranath K, Krishna Mohan GV. Removal of lead and fluoride from contaminated water using exhausted coffee grounds based bio-sorbent. *J Environ. Manage.* 2018; 218: 602-612.

Nguyen VT, Nguyen TB, Chen CW, Hung CM, Vo TD, Chang JH, et al. Influence of pyrolysis temperature on polycyclic aromatic hydrocarbons production and tetracycline adsorption behavior of biochar derived from spent coffee ground. *Bioresour. Technol.* 2019; 284: 197-203.

Peiris C, Gunatilake SR, Mlsna TE, Mohan D, Vithanage M. Biochar based removal of antibiotic sulfonamides and tetracyclines in aquatic environments: A critical review. *Bioresour. Technol.* 2017; 246: 150-159.

Rajapaksha AU, Vithanage M, Zhang M, Ahmad M, Mohan D, Chang SX, et al. Pyrolysis condition affected sulfamethazine sorption by tea waste biochars. *Bioresour. Technol.* 2014; 166: 303-8.

Rodriguez-Narvaez OM, Peralta-Hernandez JM, Goonetilleke A, Bandala ER. Treatment technologies for emerging contaminants in water: A review. *Chem. Eng. J.* 2017; 323: 361-380.

Sun P, Li Y, Meng T, Zhang R, Song M, Ren J. Removal of sulfonamide antibiotics and human metabolite by biochar and biochar/H<sub>2</sub>O<sub>2</sub> in synthetic urine. *Water*

Res. 2018; 147: 91-100.

Teixido M, Pignatello JJ, Beltran JL, Granados M, Peccia J. Speciation of the ionizable antibiotic sulfamethazine on black carbon (biochar). *Environ. Sci. Technol.* 2011; 45: 10020-7.

Tsai W-T. The potential of pyrolysing exhausted coffee residue for the production of biochar. *Handbook of Coffee Processing By-Products*, 2017, pp. 299-322.

Vardon DR, Moser BR, Zheng W, Witkin K, Evangelista RL, Strathmann TJ, et al. Complete Utilization of Spent Coffee Grounds To Produce Biodiesel, Bio-Oil, and Biochar. *ACS Sustainable Chem. & Eng.* 2013; 1: 1286-1294.

Wang T, Zhai Y, Zhu Y, Li C, Zeng G. A review of the hydrothermal carbonization of biomass waste for hydrochar formation: Process conditions, fundamentals, and physicochemical properties. *Renew. and Sustainable Energy Reviews* 2018; 90: 223-247.

Xie M, Chen W, Xu Z, Zheng S, Zhu D. Adsorption of sulfonamides to demineralized pine wood biochars prepared under different thermochemical conditions. *Environ. Pollut.* 2014; 186: 187-94.

Yu KL, Lau BF, Show PL, Ong HC, Ling TC, Chen WH, et al. Recent developments on algal biochar production and characterization. *Bioresour. Technol.* 2017; 246: 2-11.

Zhang P, Li Y, Cao Y, Han L. Characteristics of tetracycline adsorption by cow manure biochar prepared at different pyrolysis temperatures. *Bioresour.*



Technol. 2019a; 285: 121348.

Zhang Z, Zhu Z, Shen B, Liu L. Insights into biochar and hydrochar production and applications: A review. Energy 2019b; 171: 581-598.

Journal Pre-proof

**Fig. 1.** Thermogravimetric analysis for spent coffee grounds.

**Fig. 2.** Scanning electron microscope images of biochar and hydrochar.

**Fig. 3.** (a) X-ray diffraction (XRD) patterns, and Fourier transform infrared (FTIR) spectra of (b) biochar, (c) hydrochar and (d) after adsorption SDZ and SMX on biochar or hydrochar.

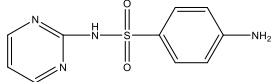
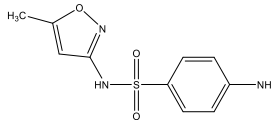
**Fig. 4.** The XPS spectra of (a) BC-400, (b) BC-500, (c) HC-6h and (d) HC-10h.

**Fig. 5.** Adsorption capacity of SDZ and SMX on (a) biochar and (b) hydrochar at 25 °C and initial concentration of 500 $\mu$ g/L.

**Fig. 6.** Adsorption isotherms for SDZ and SMX on (a) biochar and (b) hydrochar. (SDZ adsorption on BC-500 and HC-10h, SMX adsorption on BC-400 and HC-6h)

**Fig. 7.** Adsorption kinetics for SDZ and SMX on (a) biochar and (b) hydrochar. (SDZ adsorption on BC-500 and HC-10h, SMX adsorption on BC-400 and HC-6h)

**Table 1**  
Physico-chemical properties of the SDZ and SMZ

Antibiotic	Chemical structure	Molecular mass	Chemical formula	pK <sub>a</sub>	K <sub>ow</sub>	Molar refractivity
SDZ		250.28	C <sub>10</sub> H <sub>10</sub> N <sub>4</sub> O <sub>2</sub>	pK <sub>a1</sub> =2.0 pK <sub>a2</sub> =6.5	0.90	64.2
SMX		253.27	C <sub>10</sub> H <sub>11</sub> N <sub>3</sub> O <sub>3</sub>	pK <sub>a1</sub> =1.8 pK <sub>a2</sub> =5.7	0.89	64.5

**Table 2**

Retention times, parent ions, daughter ions, limit of detection, limit of quantification of SDZ and SMX

Antibiotic	Retention times(min)	Parent ions (m/z)	Daughter ions (m/z)	Limit of Detection( $\mu\text{g}/\text{kg}$ )	Limit of Quantification( $\mu\text{g}/\text{kg}$ )
SDZ	0.87	251.0	156.0 108.0	0.07	0.24
SMX	0.92	254.1	156.2 108.2	0.13	0.50

**Table 3**

Yields, ash contents, elemental compositions and pore properties of BC and HC

Sample	Yield(%)	Ash content(%)	Elemental composition							Pore properties		
			C(%)	H(%)	O(%)	N(%)	O/C	H/C	(N+O)/C	Surface area(m <sup>2</sup> /g)	Pore volume (cm <sup>3</sup> /g)	Pore diameter(nm)
BC-200	96.8	0.30	49.66	7.95	40.11	1.99	0.81	0.16	0.85	0.17	0.000599	13.87
BC-300	59.7	0.75	68.82	7.63	19.76	3.05	0.29	0.11	0.33	0.27	0.000750	10.99
BC-400	35.8	1.23	75.39	4.81	15.09	3.48	0.20	0.06	0.25	2.29	0.005641	9.87
BC-500	28.6	2.43	76.36	3.20	14.43	3.59	0.19	0.04	0.24	1.46	0.003648	10.01
BC-600	26.8	3.22	79.39	2.11	11.96	3.32	0.15	0.03	0.19	0.58	0.003108	21.43
BC-700	25.8	4.55	81.23	1.31	9.81	3.10	0.12	0.02	0.16	0.46	0.002619	22.77
HC-2	80.3	0.70	55.82	9.17	32.14	2.18	0.58	0.16	0.61	0.17	0.000261	6.24
HC-4	72.0	0.35	57.06	9.21	31.39	2.00	0.55	0.16	0.59	0.26	0.000609	9.40
HC-6	67.1	0.33	58.77	9.16	29.78	1.96	0.51	0.16	0.54	0.33	0.000698	8.41
HC-8	65.5	0.51	59.03	9.12	29.44	1.91	0.50	0.15	0.53	0.36	0.000716	7.97
HC-10	64.7	0.30	59.58	9.29	28.89	1.94	0.48	0.16	0.52	0.93	0.004278	18.35
HC-12	64.5	0.44	59.99	8.97	28.74	1.87	0.48	0.15	0.51	1.29	0.005592	17.38

BC and HC represent biochar and hydrochar derived from spent coffee grounds, respectively.

**Table 4**

Parameters of Freundlich and Langmuir models for SDZ and SMX adsorption by BC and HC

Adsorbent	SDZ		Adsorbent	SMX	
	Langmuir	Freundlich		Langmuir	Freundlich
BC-500	$Q_m=221.9 \mu\text{g/g}$	$K_F=12.284 \mu\text{g}^{1-n} \text{L}^n/\text{g}$	BC-400	$Q_m=481.6 \mu\text{g/g}$	$K_F=8.885 \mu\text{g}^{1-n} \text{L}^n/\text{g}$
	$K_L=6 \times 10^{-3} \text{L}/\mu\text{g}$	$n=0.399$		$K_L=3 \times 10^{-3} \text{L}/\mu\text{g}$	$n=0.544$
	$r^2=0.978$	$r^2=0.936$		$r^2=0.974$	$r^2=0.994$
HC-10h	$Q_m=295.1 \mu\text{g/g}$	$K_F=3.286 \mu\text{g}^{1-n} \text{L}^n/\text{g}$	HC-6h	$Q_m=740.6 \mu\text{g/g}$	$K_F=1.437 \mu\text{g}^{1-n} \text{L}^n/\text{g}$
	$K_L=2 \times 10^{-3} \text{L}/\mu\text{g}$	$n=0.579$		$K_L=7 \times 10^{-4} \text{L}/\mu\text{g}$	$n=0.773$
	$r^2=0.999$	$r^2=0.982$		$r^2=0.999$	$r^2=0.995$

**Table 5**

Kinetic parameters of Pseudo-first order, Pseudo-second order for SDZ and SMX adsorption by BC and HC.

Adsorbent	Pseudo-first-order model			Pseudo-second-order model			$\Delta G_0(\text{kJ/mol})$
	$q_e(\mu\text{g/g})$	$k_1(\text{h}^{-1})$	$r^2$	$q_e(\mu\text{g/g})$	$k_2(\text{g } \mu\text{g}^{-1}\text{h}^{-1})$	$r^2$	
BC-400 <sup>a</sup>	130.83	1.101	0.882	136.75	0.012	0.992	-4.65
BC-500 <sup>b</sup>	119.43	0.549	0.951	126.69	0.007	0.999	-3.59
HC-6h <sup>a</sup>	84.01	1.630	0.938	86.84	0.031	0.988	-0.71
HC-10h <sup>b</sup>	85.10	0.173	0.978	95.16	0.002	0.998	-0.48

<sup>a</sup> Adsorbate was SMX

<sup>b</sup> Adsorbate was SDZ

Graphical abstract

**highlights**

- BC and HC were produced from spent coffee ground by pyrolysis and HTC, respectively.
- BC owned higher carbonization and less oxygen-containing functional groups than HC.
- BC exhibited a higher maximum adsorption capacity for sulfonamide than HC.
- For BC, adsorption was mostly governed by  $\pi$ - $\pi$  electron donor-acceptor interactions.
- Hydrogen bonds played the key role in sulfonamide antibiotics adsorption for HC.



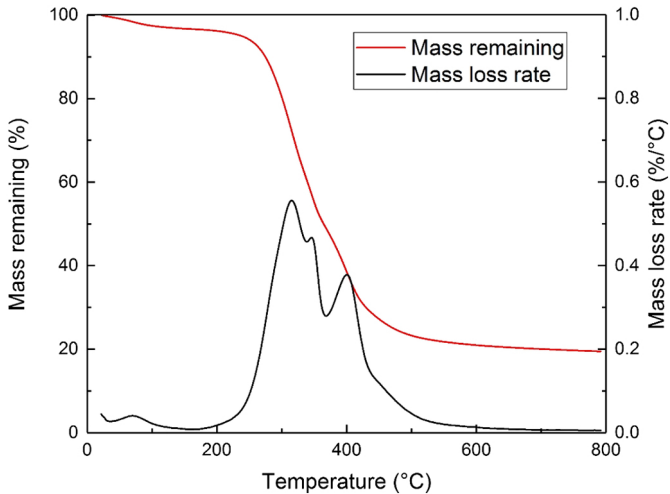


Figure 1

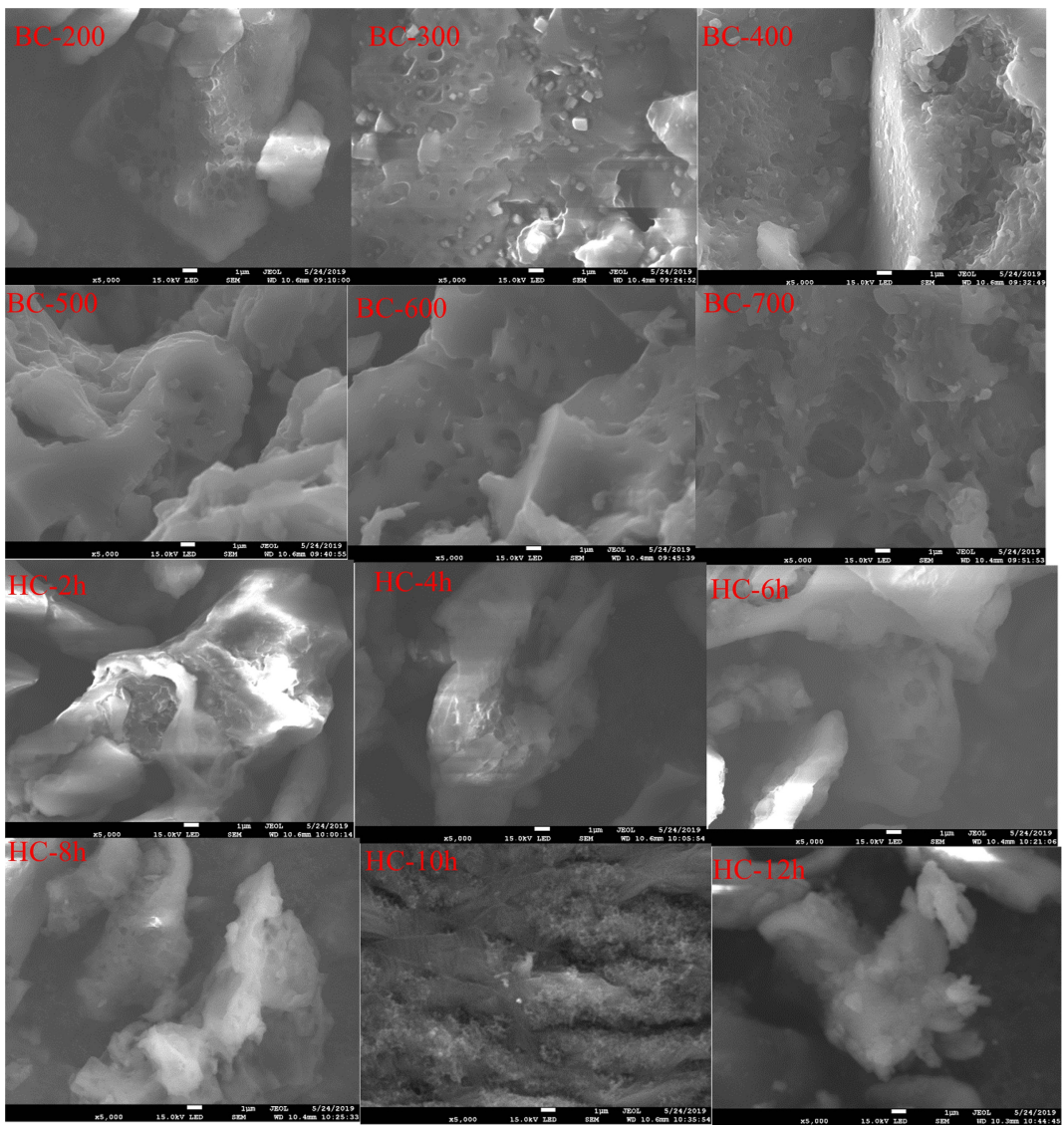
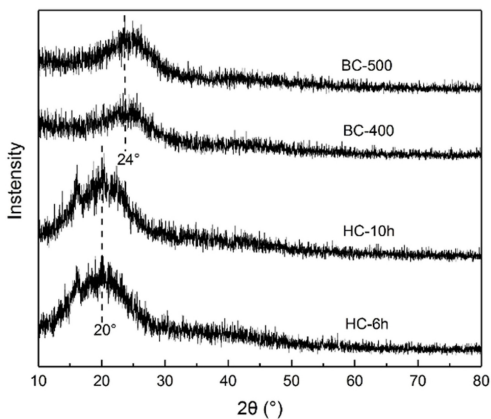
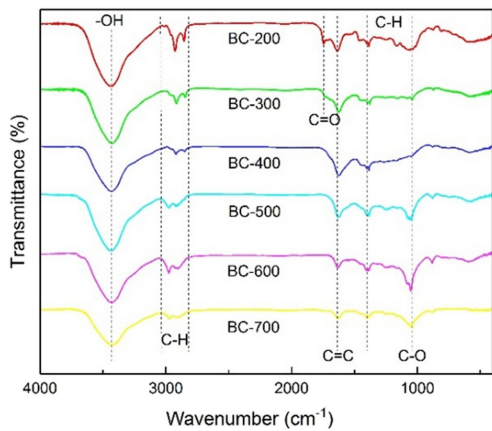


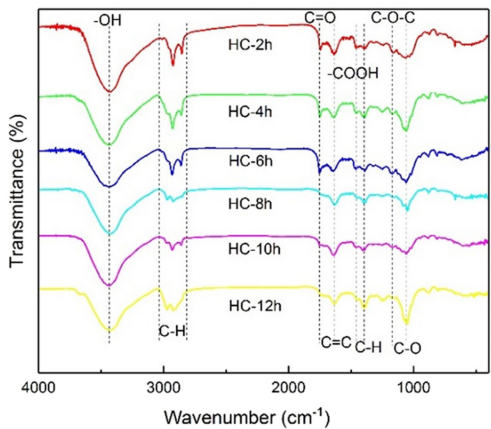
Figure 2



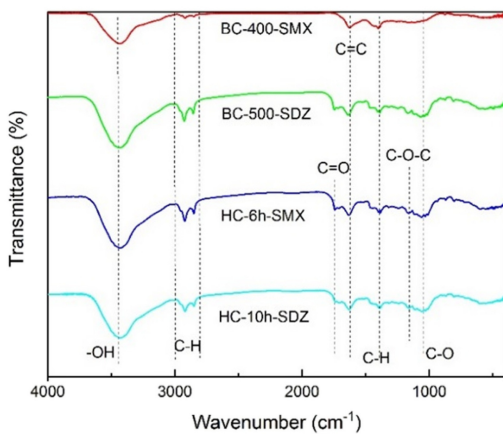
(a)



(b)



(c)



(d)

Figure 3

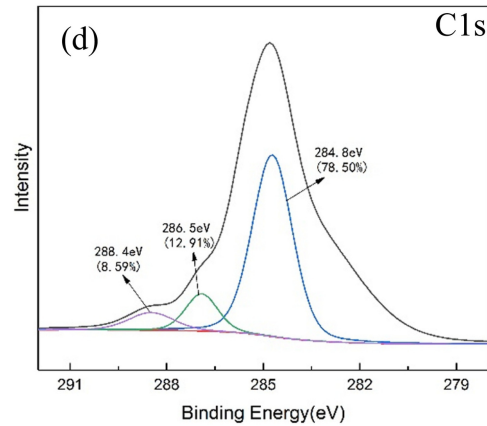
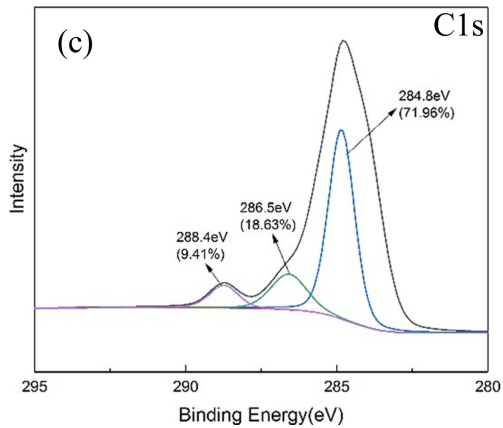
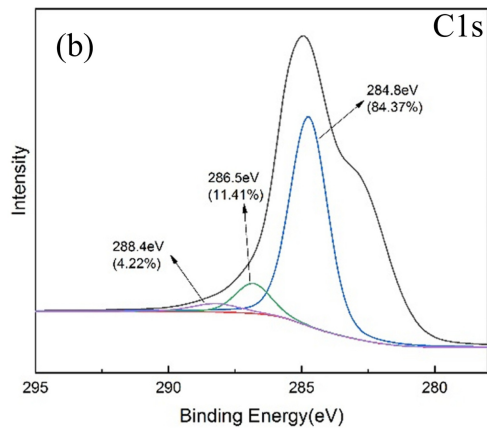
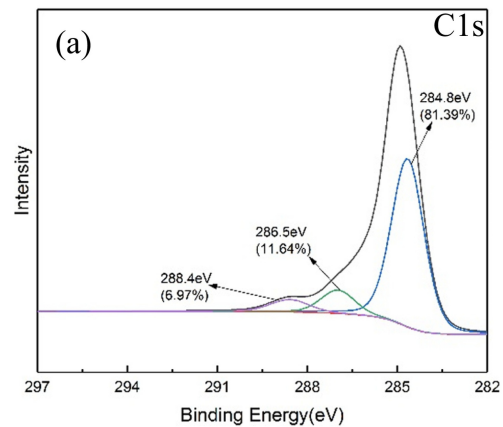
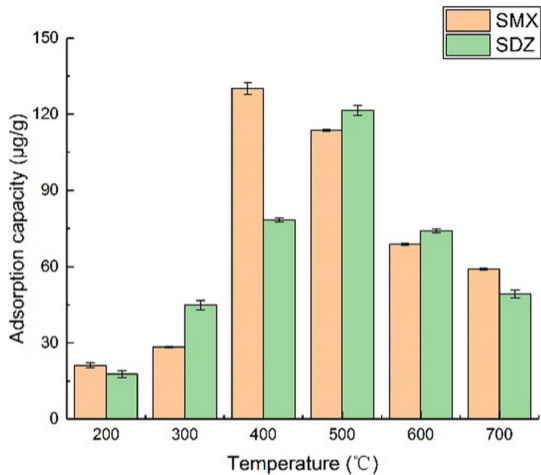
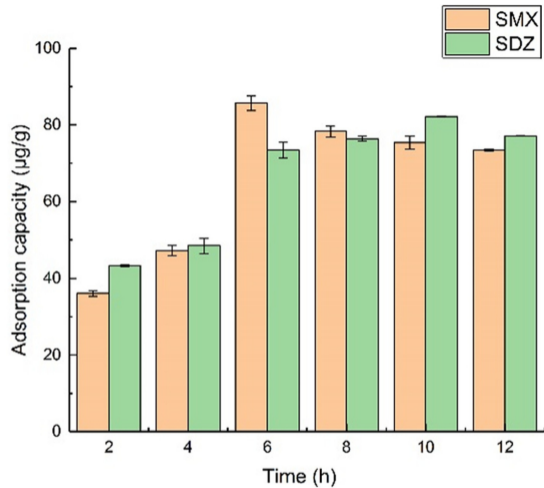


Figure 4

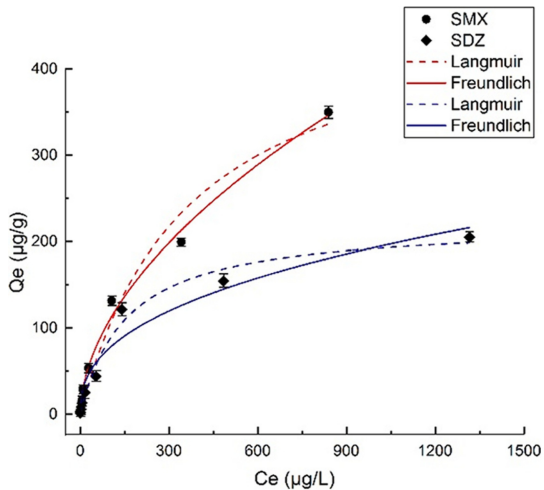


(a)

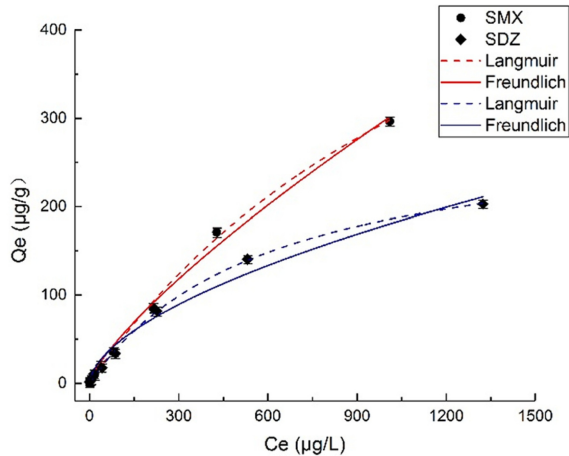


(b)

Figure 5

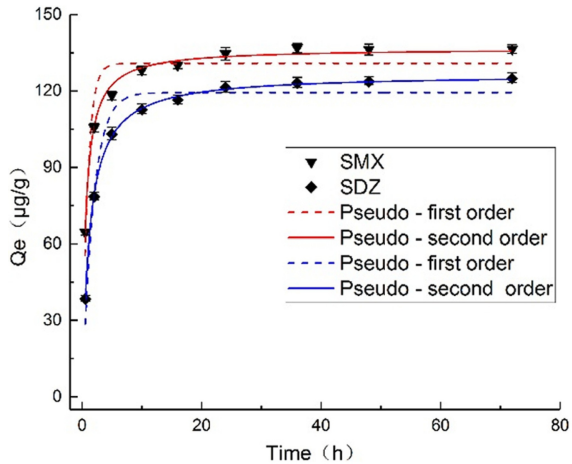


(a)

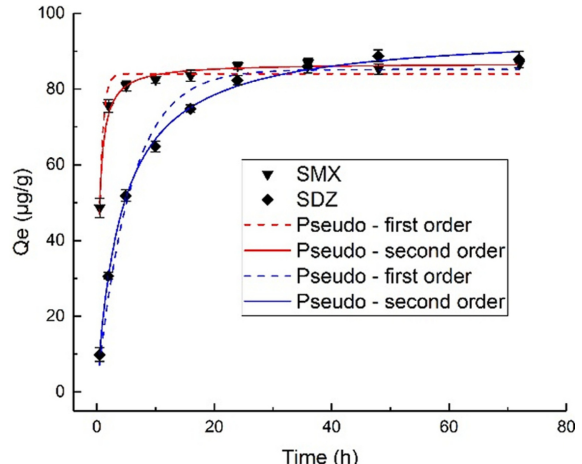


(b)

Figure 6



(a)



(b)

Figure 7